# In the Hunt for Therapeutic Targets: Mimicking the Growth, Metastasis, and Stromal Associations of Early-Stage Lung Cancer Using a Novel Orthotopic Animal Model

*Ido D. Weiss, PhD,* Ezra Ella, PhD,* Omri Dominsky, BA,* Yoav Smith, PhD,* Michal Abraham, PhD,* Hanna Wald, PhD,* Zippora Shlomai, MSc,† Gideon Zamir, MD,† Sara W. Feigelson, PhD,‡ Elias Shezen, PhD,‡ Amir Bar-Shai, MD,‡ Ronen Alon, PhD,‡ Uzi Izhar, MD,§ Amnon Peled, PhD,* Oz M. Shapira, MD,§ and Ori Wald, MD, PhD*§*

**Background:** The existing shortage of animal models that properly mimic the progression of early-stage human lung cancer from a solitary confined tumor to an invasive metastatic disease hinders accurate characterization of key interactions between lung cancer cells and their stroma. We herein describe a novel orthotopic animal model that addresses these concerns and consequently serves as an attractive platform to study tumor–stromal cell interactions under conditions that reflect early-stage lung cancer.

**Methods:** Unlike previous methodologies, we directly injected small numbers of human or murine lung cancer cells into murine's left lung and longitudinally monitored disease progression. Next, we used green fluorescent protein-tagged tumor cells and immuno-fluorescent staining to determine the tumor's microanatomic distribution and to look for tumor-infiltrating immune cells and stromal cells. Finally, we compared chemokine gene expression patterns in the tumor and lung microenvironment.

**Results:** We successfully generated a solitary pulmonary nodule surrounded by normal lung parenchyma that grew locally and spread distally over time. Notably, we found that both fibroblasts and leukocytes are recruited to the tumor's margins and that distinct myeloid cell attracting and CCR2-binding chemokines are specifically induced in the tumor microenvironment.

**Conclusion:** Our orthotopic lung cancer model closely mimics the pathologic sequence of events that characterizes early-stage human lung cancer propagation. It further introduces new means to monitor tumor–stromal cell interactions and offers unique opportunities to test therapeutic targets under conditions that reflect early-stage lung cancer. We argue that for such purposes our model is superior to lung cancer models that are based either on genetic induction of epithelial transformation or on ectopic transplantation of malignant cells.

**Key Words:** Non–small-cell lung cancer, Lung, Orthotopic animal model, Tumor microenvironment.

(*J Thorac Oncol.* 2015;10: 46–58)

Lung cancer is the second most common malignancy and the leading cause of cancer-related death in the United States and throughout the world.[1] Out of all lung cancer cases, patients who are diagnosed with early-stage disease (stages IA–IIB) have the best prognosis.[2] These patients are considered to have a solitary pulmonary tumor that has not yet metastasized and, therefore, are referred to surgery which is considered to be the best therapeutic approach.[3] Nonetheless, about 50% of these patients eventually succumb to the disease due to either local recurrence of the tumor or to its metastatic spread.[2,3] To be able to develop innovative therapeutics for these patients, novel insights into the processes that govern the growth and metastasis of early-stage lung cancer are urgently needed.[4–6] In particular, it is important to study the interactions of lung cancer tumor cells with their native lung microenvironment and to try and understand how these processes regulate tumor growth and spread.[7–9] Unfortunately, the study of these critical issues is hampered, in part, by the lack of an appropriate animal model that accurately mimics the pathologic sequence of events that characterizes early-stage human lung cancer: a single pulmonary nodule that is surrounded by normal lung parenchyma and that, over time, locally grows and forms metastasis.[10–12]

More specifically, existing lung cancer models fall into two main categories, and both do not allow accurate mimicry of lung caner disease progression. One set of models is based on the induction of epithelial transformation, either by the administration of a chemical carcinogens or by genetically regulating the expression of a specific oncogenes or tumor suppressor genes in the lung.[13] For example, exposure of mice

*Goldyne Savad Institute of Gene Therapy, Hadassah University Hospital, Jerusalem, Israel; †Laboratory for Surgical Research, Hadassah University Hospital, Jerusalem, Israel; ‡Department of Immunology, Weizmann Institute of Science, Rehovot, Israel; and §Department of Cardiothoracic Surgery, Hadassah University Hospital, Jerusalem, Israel.

Disclosure: This work was supported by the Israeli Science Foundation Morasha research grant program (#1755/11). R.A. was supported by FAMRI—the Flight Attendant Medical Research Institute Foundation. The remaining authors have no conflict of interest to declare.Drs. Weiss and Ella contributed equally to this work.

Address for Correspondence: Ori Wald, MD, PhD, Department of Cardiothoracic Surgery, Hadassah University Hospital, PO Box 12000, Jerusalem, Israel. E-mail: ori.wald@mail.huji.ac.il

DOI: 10.1097/JTO.0000000000000367



ISSN: 1556-0864/15/1001-0046

to the tobacco-specific carcinogen 4-(methylnitrosamino)-1-(3-pyridyl)-1-butanone induces the activation of multiple pro-proliferative signaling pathways such as ERK1/2, PKC, PI3K/Akt, and MAPK, that eventually lead to lung tumorigenesis.[14] Alternatively, lung epithelial transformation may be stimulated either by enhancing the expression of a tumor driving mutation such as K-RAS or by silencing the expression of a tumor suppressor genes such as P53 in the lung parenchyma.[15,16] An important advantage of the genetic approach is that it facilitates the characterization of single tumor-promoting pathways under regulated conditions and also permits the testing of pathway-specific inhibitors as potential new drugs.[17] Nonetheless, one of the most frequent criticisms about epithelial transformation-based lung cancer models is that they inherently modify the entire lung microenvironment and also induce the formation of multiple bilateral tumors that only rarely recapitulate the metastatic phenotype seen within human tumors.[18] As such, these models limit the potential to assess how a solitary lung tumor interacts with the native lung microenvironment and how, for example, such a tumor metastasizes to the contralateral lung. Further limitations of such models are related to the long time elapsed till tumor formation, the relative complexity of the modeling system, and the high cost of some of these models.[19,20]

The second set of approaches used to model lung cancer is based on ectopic delivery of either cancerous cell lines or of patient-derived tumor xenografts. And yet, these models display other kinds of limitations. For example, cancerous cell line-based models require the injection of very large number of cells, which, as a result, can overwhelm and escape the normal immune response against primary tumors.[21] This large volume of cells may also induce a rapid and extensive inflammatory response which masks the physiologic events that accompany initial phase tumors.[21] Another important issue to consider with regard to the ectopic approach is to do with the method and site of tumor induction. For example, tail-vein injection of the cancerous cells is associated with spread of the cells to the entire organism and with the generation of multiple tumors (Supplementary Figure 1, Supplemental Digital Content 1, http://links.lww.com/JTO/A712). Therefore, although this approach can be used to probe tumor metastasis to the lung, it cannot be used to study tumor formation in the lung.[10,11,22] Also problematic is the subcutaneous administration of the cancerous cells or the subcutaneous implantation of human-derived tumor xenografts, which by definition introduces the cells to a microenvironment that is totally different from the tumors original microenvironment. Collectively, although the above-described experimental approaches have provided many important molecular insights into the process of lung cancer initiation and into the process of non-lung cancer malignant tumor cell metastasis to the lung, they fall short in providing an appropriate system to probe how a single pulmonary nodule propagates in the native lung microenvironment and how it spreads to secondary organs.[10–12]

In light of these considerations, we reasoned that orthotopic transplantation of lung cancer cells might overcome some of these limitations. Although several previous attempts with this approach have been made, they have all been only partially successful due to technical limitations that prevented the generation of a single pulmonary nodule that was anatomically confined to the lung and that, over time, locally grew and spread in a manner that resembles the growth and metastasis of human non–small-cell lung cancer (NSCLC).[23,24] In this article, we address these concerns and describe a novel and refined orthotopic animal model that can, consequently, serve as an attractive platform to study the crosstalk between tumor cells and the lung microenvironment. Distinct from previous methodologies, our approach involves stereotactic-guided injection of a minute number of cells in the microliter range of volumes, directly into the left lobe of the murine lung. Mimicking real disease progression, this novel orthotopic approach allowed us to successfully generate a solitary microscopic pulmonary nodule that is surrounded by normal lung parenchyma and to systematically follow its growth and spread for a period of 1 to 6 weeks. This methodology further enabled us for the first time to introduce an animal model in which a solitary lung tumor metastasizes from the lung to secondary organs such as the contralateral lung and liver. Finally, in search of key pathways that might contribute to tumor progression, the model also allowed us to identify certain chemotactic molecules and distinct populations of fibroblasts and myeloid cells that may serve as potential therapeutic targets for lung cancer therapy.

## MATERIALS AND METHODS

### Cell Lines

The human H460 (large cell carcinoma) and A549 (adenocarcinoma) cell lines as well as the murine 3LL (also known as Lewis lung carcinoma) cell line were all purchased from American Type Culture Collection (Manassas, VA) and were maintained in RPMI (Gibco Laboratories, Grand Island, NY) containing 10% fetal calf serum, 1 mM L-glutamine, 100 U/ml penicillin, and 0.01 mg/ml streptomycin (Biological Industries, Kibbutz Beth Haemek, Israel). All cell lines were tested for mycoplasma contamination and were found to be negative.

### In Vivo Experimental Design

For experiments in the syngeneic system, we injected 3LL cells to C57BL/6 immune-competent mice. For experiments in the humanized system, we injected H460 and A549 cells (human lung cancer cells) to NSG immune-deficient mice.

- To calibrate the model, 15 C57BL/6 were injected with 250, 500, or 1000 3LL cells (five mice per group). To assess for tumor formation, mice were killed after 3 weeks.
- To assess the ability of micro-positron emission tomography/computed tomography (PET/CT) to detect the tumors, five C57BL/6 were injected with 500 3LL cells and imaging was performed 3 weeks after tumor cell implantation.
- To assess the tumor histology, 1 week after tumor cell injection, five C57BL/6 were injected with 500 3LL cells and killed at the indicated time point.
- For the immuno-fluorescent staining, 10 C57BL/6 were injected with 500 GFP-tagged 3LL cells. The mice were

 

killed (five mice per group) 1 and 3 weeks after tumor cell implantation.
- For the analysis of tumor-infiltrating and lung leukocytes, five C57BL/6 were injected with 500 3LL cells. Mice were killed 3 weeks after tumor cell implantation. Next, the tumor-infiltrating and lung resident leukocytes were extracted as described below. This experiment was repeated three times; thus, the total number of injected mice was 15.
- For the gene-chip analysis and quantitative polymerase chain reaction (qPCR), five C57BL/6 were injected with 500 3LL cells and the mice were killed 3 weeks after tumor cell implantation.
- To assess for the production of CCL2 and CCL7 in the tumors, five C57BL/6 were injected with 500 GFP-tagged 3LL cells. The mice were killed 3 weeks after tumor cell implantation. Three control non-tumor-bearing mice were also killed.
- For the immunohistochemistry staining, 5 C57BL/6 were injected with 500 GFP-tagged 3LL cells. The mice were killed 3 weeks after tumor cell implantation.
- To assess for tumor formation by H460 cells, 12 NSG mice were injected with $7.5 \times 10^3$ or $10^4$ H460 cells (six mice per group) and mice were killed after 6 weeks.
- To assess for tumor formation by A549 cells, five NSG mice were injected with $5 \times 10^3$ A549 cells and mice were killed after 6 weeks.

## Detailed Description of the Surgical Procedure

Cultured H460, A549 ($5 \times 10^3$ or $10^4$ per 1 μl), and 3LL (250, 500, or 1000 per 1 μl) cells were harvested and suspended in RPMI-1640 (BD Bioscience, NJ). Before injection, the cells were mixed with matrigel (BD Bioscience) at 1:1 ratio and kept on ice until injection. For injection, the cell mixture was gently mixed and transferred into a 10-μl syringe (Hamilton, NV, USA) fitted with a 31-gauge needle. The syringe was loaded on the stereotactic injection system, and 2 μl of cell mixture was injected to each mouse.

Mice were anesthetized using ketamine/xylasine and the fur covering the left thorax was shaved. The mice were then positioned in the lateral decubitus position with the left chest facing up and a small (0.5–1 cm) incision was made over the skin just below the scapula. Next, the chest wall muscles were gently spread until the intercostal space and pleura were clearly visible. Then, the ribs were counted from the lower border of the rib cage upward, and the site of tumor injection between the fourth and fifth ribs at the posterior axillary line was determined. At this stage, the syringe was gently advanced until its tip finely touched the intercostal space. The syringe was then advanced 3.5 mm into the lung parenchyma and the tumor cell mixture was injected. After injection of the cells, the syringe was withdrawn from the tissue and the covering muscles and skin were closed. Subsequently, mice were given an analgesic medication and were allowed to recover in a preheated incubator for 20 to 30 minutes.

Lung harvesting was performed as follows: mice were first euthanized by overdose injection of ketamine/xylasine. Next, the chest cavity was exposed and the lungs perfused with 4% buffered paraformaldehyde through the trachea. For frozen section preparation, the lungs were perfused with 2% buffered paraformaldehyde through the trachea and frozen in OCT.

The animal care and use committee at Hadassah University Hospital approved the experimental protocol used in this article.

## Micro-PET/CT Imaging

One hour before micro-PET/CT scanning, tumor-bearing mice were tail-vein injected with 200 uCi 18F-Fluorodeoxyglucose. All acquisitions were carried out using the Inveon multimodality PET/CT small animal-dedicated scanner (Siemens Medical Solutions, USA Inc.). Emission sinograms were normalized and corrected for attenuation, randoms, dead time, and decay. Image reconstruction was performed using Fourier rebinning and two-dimensional ordered-subsets expectation maximization, with a voxel size of $0.776 \times 0.776 \times 0.796\,mm^3$. Image analysis was performed using Inveon Research Workplace 3.1 (Siemens Medical Solutions, USA Inc.).

## Histology, Hematoxylin and Eosin, Fluorescent Immuno-Staining, and Immunohistochemistry Staining

Tissue samples of control lungs and tumor-bearing lungs were routinely fixed with formalin and embedded in paraffin. Tissues were then serially sectioned in 4 to 7 μM distances and transferred to slides for hematoxylin and eosin staining.

For immuno-fluorescent staining, the following antibodies were used: GFP was amplified by chicken polyclonal antibodies to GFP (ab13970; Abcam, Cambridge, England, United Kingdom) followed by Alexa 488 donkey anti-chicken secondary antibodies (Jackson, 703-545-155). Rabbit pAb to S100A4 (ab27957; Abcam) followed by Alexa 647 donkey anti-rabbit secondary antibodies (Jackson, 711-605-152; JAX Mice, Clinical & Research Services, Bar Harbor, ME) and PE-conjugated anti-mCD45 (clone 30-F11, Biolegend, San Diego, CA). For immunohistochemistry, slides were incubated with anti-CD45 (Abcam, ab10558) or anti-aSMA (DAKO M0851). 3-Amino-9-ethylcarbazole was used for color development and sections were counterstained with hematoxylin.

## Isolation of Tumor-Infiltrating Leukocytes (CD45+)

Three weeks after injection of 3LL cells to C57BL/6 mice, the mice were killed and the lungs were perfused by injection of saline to the right heart ventricle. Next, the lungs were harvested and the left lobe tumors were carefully dissected from the left lung parenchyma. The right lung lobes were used as a non-tumor-bearing control sample. In each experiment, the tumor and lung samples from five mice were pooled together to yield a large number of leukocytes. Both lung and tumor specimens were roughly minced and put in RPMI containing collagenase IV and DNase (200 μg/ml and 5 μg/ml, respectively, both from Worthington, Lakewood, NJ) for 40 minutes at 37°C. Afterward, samples were meshed through a 70-μm disposable mesh (Falcon, BD Bioscience) and washed twice with phosphate buffered saline (wash buffer) containing 4% FBS (Biological Industries). Samples were

reconstituted in 100-µl wash buffer, blocked with 1% mouse serum, and separated using anti-mouse CD45 magnetic beads (Miltenyi, Germany) as described by the manufacturer.

### Flow Cytometry

Isolated tumor-infiltrating cells and lung resident cells were stained with eFluor450-labeled anti-CD45.2, APC-labeled anti-CD11b, and FITC-labeled anti-Gr-1. All antibodies were purchased from eBioscience (San Diego, CA). Next, the cells were washed twice with PBS and then stained for dead cells with the Dead Cell Marker (Invitrogen, Grand Island, NY). Cells were acquired on a LSR-II flow cytometer (BD Bioscience) and thereafter analyzed using FlowJo software (Tree Star, Ashland, OR).

### Gene-Chip Protocol

Total RNA was extracted from normal lung tissue, 3LL tumor tissue, and from 3LL cells growing in culture. The RNA was subjected to gene expression profiling using GeneChip Mouse Gene 1.0 ST Array (Affymetrix, Santa Clara, CA) according to the manufacturer's protocol.

### Quantitative PCR Analysis

Quantitative PCR analysis of the expression of the chemokines CXCL-2, 3, 12, 16 and CCL-2, 3, 5, 7, 17, 22 was performed using TaqMan technology (Applied Biosystems and Invitrogen). TaqMan fast universal PCR master mix and specific primers were purchased from the company and the experiment was performed according to the manufacturer's instructions. For each tissue sample, the experiment was performed in triplicate.

### Enzyme-Linked Immunosorbent Assay

3LL-derived lung tumors and control normal lung tissue samples were homogenized in Greenberger Lysis Buffer containing 300 mM NaCl,15 mM Tris, 2 mM $MgCl_2$, 2 mM Triton (X-100), and protease inhibitors (Complete Mini Roche diagnostic GmbH, Mannheim, Germany, Ref 11836153001) one tablet per 10 ml. One milligram of tissue was homogenized in 20 µl lysis buffer. After homogenization, the suspension was centrifuged and CCL2 and CCL7 were determined in the supernatant by enzyme-linked immunosorbent assay (ELISA) according to the manufacture's instructions. For CCL2, the Quantikine ELISA kit (R&D systems Inc., Minneapolis, MN) was used. For CCL7, the instant ELISA kit by eBioscience/bender medsystems (Vienna, Austria) was used. Protein content in each tissue sample was determined by Bradford assay and the chemokine content in each sample was then calculated relative to the protein content in the sample to yield chemokines expressed in picograms per milligram of protein scale.

## RESULTS

### Intra-Parenchymal Injections of Minute Numbers of Murine Lung Cancer Cells Successfully Generate a Single Pulmonary Nodule that is Detectable by PET/CT

In the first set of experiments, we aimed to generate a single pulmonary nodule by injecting very small numbers of murine lung cancer cells (3LL) directly into the left lung parenchyma. We targeted the murine left lung because in this species, the left lung consists of only one lobe, hence assuring the accurate delivery of the malignant cells to a distinct anatomic compartment (Fig. 1*A*). In addition, in an attempt to reduce potential tissue damage and to prevent spillage of cells from the lung to the thoracic cavity, we used a very fine needle and suspended the cells with matrigel to a total volume of injection of 2 µl, a volume that represents only about 0.5% of the left lung volume. To calibrate the rate of tumor formation, we injected dosages of 250, 500, or 1000 murine 3LL lung carcinoma into the left lung of C57BL/6 mice and 3 weeks later killed the mice. Pulmonary nodules formed in 60% (3 of 5), 80% (4 of 5), and 100% (5 of 5) of mice injected with 250, 500, and 1000 cells, respectively. Importantly, as shown in Figure 1*B*, the mice developed a single pulmonary nodule and no chest wall tumor or mediastinal masses were observed. When keeping tumor-bearing mice alive for 4 weeks, the 3LL tumors tended to outgrow from the lung and to invade the tumor adjacent chest wall (data not shown). At this time point, the mice showed reduction in body weight and reduced mobility and thus in further experiments, we did not keep tumor-bearing mice alive for more than 3 weeks. Next, we tested whether micro-PET/CT imaging could detect the pulmonary nodule in live anesthetized mice. As expected, and as shown in Figure 1*C–E*, both the CT and PET modalities clearly demonstrated the pulmonary nodule in the left lung, thereby supporting the notion that the tumor is localized to a single locus.

### Orthotopically Implanted 3LL Cells Display a Locally Aggressive Growth Pattern Mimicking the Growth of Invasive Stage I Human NSCLC

In the next phase of the article, we set to determine the tumor's microscopic characteristics and to confirm that indeed a single pulmonary nodule is formed after tumor implantation. To this end, histologic serial sections were prepared from the lungs of mice injected with 500 3LL cells and killed at 1 and 3 weeks after tumor cell implantation. As can be seen in Figure 2*B*, microscopic examination of slides from the 1-week time point indicated the formation of a solitary small tumor that was surrounded by normally appearing lung parenchyma. Similarly, examination of slides from the 3-week time point also indicated the formation of a singular tumor. However, as expected at this time point, the tumor was much larger and exerted mass effects on the tumor surrounding lung parenchyma (Fig. 2*C*). Focusing on areas of interface between the 3-week-old tumor and the lung parenchyma, we found that the 3LL tumor cells invaded neighboring alveolai and also engulfed pulmonary vascular structures (Fig. 2*D*). In addition, we noticed the remarkable accumulation of leukocyte infiltrates at areas of interface between the tumor and tumor adjacent lung parenchyma as well as around blood vessels in the tumor vicinity (Fig. 2*D* and Supplementary Figure 2A and 2B, Supplemental Digital Content 2, http://links.lww.com/JTO/A713).

To further validate the surgical technique and confirm that indeed only a solitary tumor focus was formed, we next

 

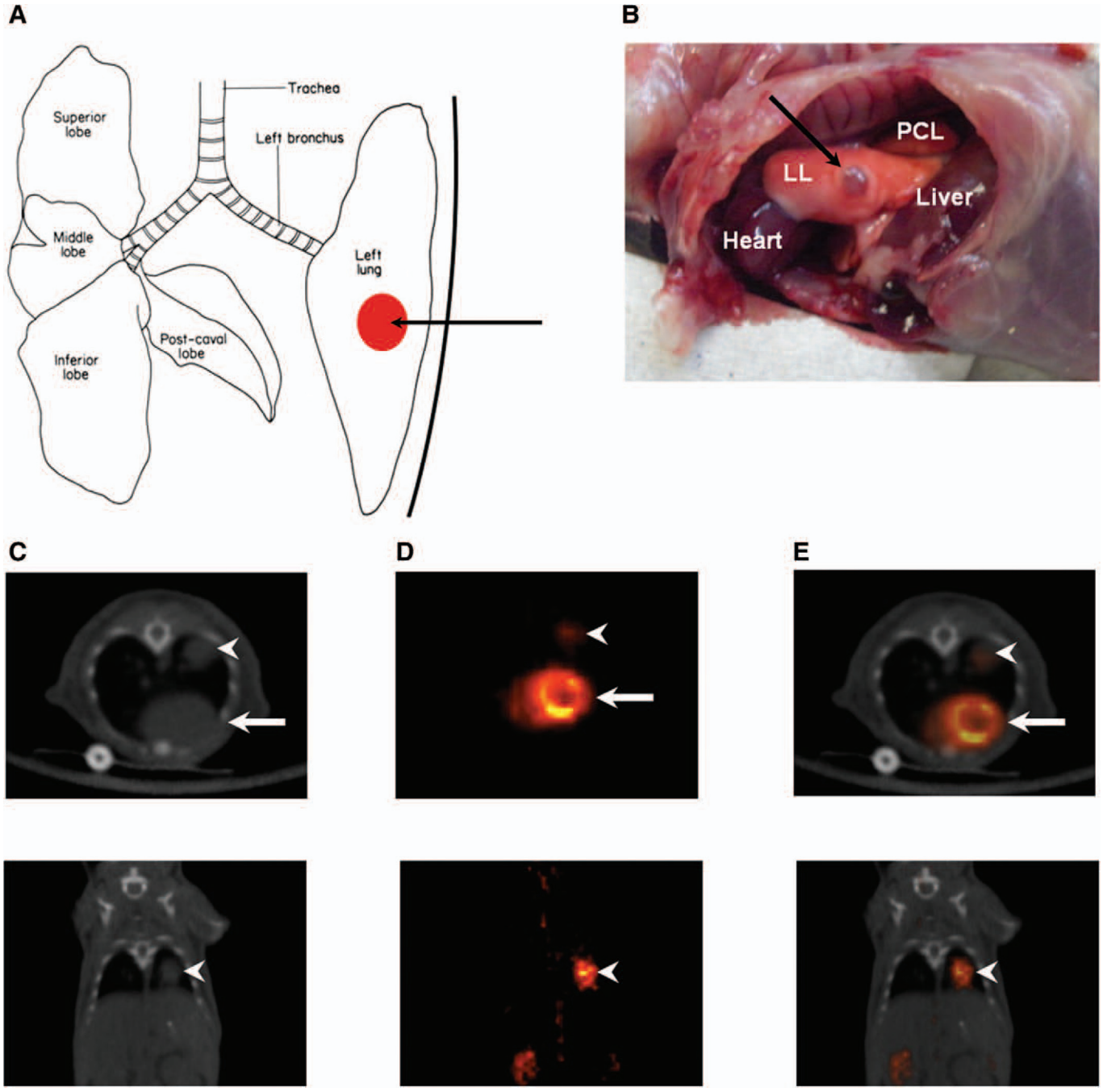


**FIGURE 1.** *A,* Schematic illustration of the anatomy of the murine lung indicating the existence of a single left lung lobe. The black line represents the pleura and the black arrow and red circle indicate trans-pleural injection of tumor cells into the left lung parenchyma. *B,* Representative image of the chest of a C57BL/6 mouse that was killed 3 weeks after injection of 500 3LL cells directly into the left lung. The black arrow points to a macroscopic single pulmonary nodule in the left lung. LL, left lung; PCL, postcaval lobe of right lung. *C–E,* Representative micro-PET/CT imaging of a C57BL/6 mouse 3 weeks after injection of 3LL cells directly into the left lung. *A,* CT sections, (*B*) PET sections, and (*C*) PET/CT superposition. Upper panels show axial sections and lower panels show coronal reconstructions. Arrowheads mark the tumor and arrows point to the heart. PET/CT, positron emission tomography/computed tomography.

followed the growth of GFP-tagged 3LL cells in vivo. As anticipated, microscopic examination of the left lung at 1 and 3 weeks after tumor cell injection confirmed the generation of a singular tumor in the left lung field (Fig. 2*E, F*). Remarkably, no GFP-positive cells were detected at sites distant from the primary tumor focus (Fig. 2*E, F*) or in remote lobes (data not shown), thus indicating that no individual cancer cells were shed from the original solitary tumor. Collectively,

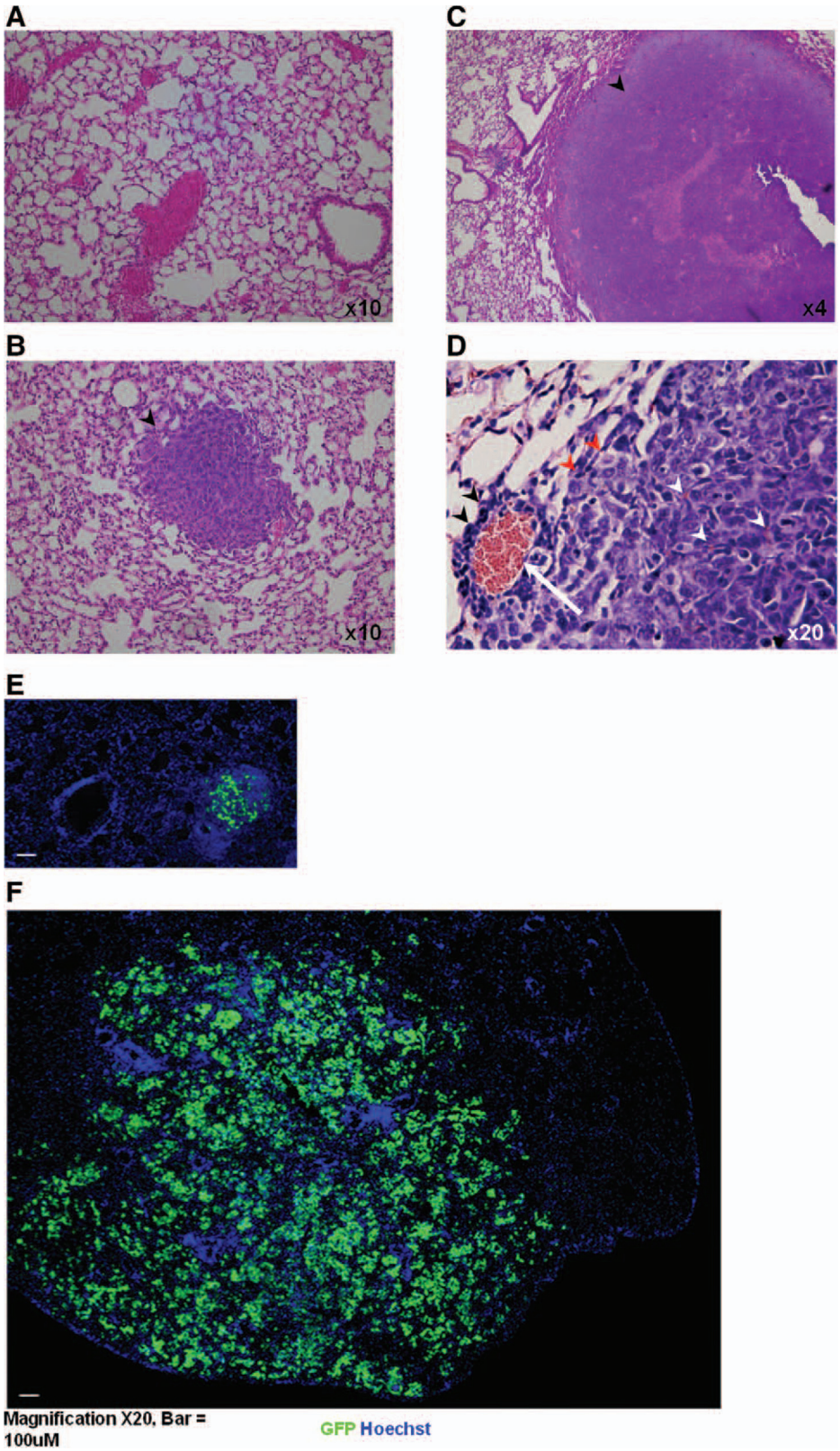


**FIGURE 2.** *A–D,* Representative histologic sections from the lungs of C57BL/6 mice that were killed 1 and 3 weeks after injection of 3LL (Lewis lung carcinoma cells) into the left lung. *A,* Control noninjected lung (magnification, ×10); (*B*) tumor 1 week after injection (magnification, ×10); (*C*) tumor 3 weeks after injection (magnification ×4); (*D*) tumor 3 weeks after injection. Red arrowheads indicate tumor cells that invade the alveolar space at the tumor periphery and black arrowheads indicate immune cells surrounding a large vessel (arrow) in tumor periphery; note that tumor cells begin to engulf the vessel, white arrowheads point to small microvessels inside the tumor (magnification ×20). *E* and *F,* Representative immuno-fluorescent staining of histologic frozen sections from the lungs of C57BL/6 mice killed 1 and 3 weeks after injection of 500 GFP-expressing 3LL cells into the left lung. Green: anti-GFP staining, blue: Hoechst nuclear staining. Bar = 100 μm. *E,* Tumor cells were visualized by anti-GFP staining of the left lung 1 week after injection and (*F*) tumor cells were visualized by anti-GFP staining of the left lung 3 weeks after injection.

these observations validate the solitary nature of our orthotopic model and further suggest that the 3LL tumors display a locally invasive growth pattern that mimics the behavior of locally invasive stage I human NSCLC.

## 3LL Cells Recruit Fibroblasts and Distinct Populations of Leukocytes to Their Vicinity during Tumor Progression

To further elucidate the composition of stromal lung cells within and nearby the growing tumor, we next stained either the tumor or lung areas remote from the tumor for markers of two main cell populations known to comprise the tumor stroma: (1) lung fibroblasts (identified by the lung fibroblast marker, S100A4[25] and by aSMA)[26] and (2) leukocytes (identified by CD45). Notably, 1 week after tumor implantation, no S100A4-positive cells could be found inside or nearby GFP-labeled tumor cells; 2 weeks later, as the tumor grew, a thin layer of S100A4-positive cells appeared at the margin of the growing tumor, with a negligible number of S100A4-positive cells detected at lung sections distant to the tumor (Fig. 3*A–C*). Given that some malignant cells including lung cancer cells can also express the S100A4 marker and to exclude the possibility that all S100A4-positive cells were tumor cells, we examined our staining at a higher degree of magnification[27,28] As shown in Figure 3*D*, multiple S100A4-positive cells at the tumor edge were GFP negative suggesting that these were cancer-associated fibroblast. In addition, some of the S100A4 cells were also positive for GFP indicating that these are S100A4-expressing tumor cells. To further solidify the observation that fibroblasts were recruited to the tumor edge, we next stained tumor sections for an additional cancer-associated fibroblast marker: aSMA, as expected we found that aSMA-positive cells were indeed abundant in the tumor margin. Notably, some aSMA-positive cells were also detected in the tumor bulk indicating recruitment of these cells not only to the tumor edge but also to the tumor parenchyma (Supplementary Figure 3A, Supplemental Digital Content 3, http://links.lww.com/JTO/A714).[26]

In addition to fibroblasts, we also found that the density of leukocytes (CD45+ cells) in the margin of the 3-week-growing tumor was significantly higher than in remote lung areas distant to the tumor (Fig. 4*A, B*). Notably, the density of these CD45+ cells in areas distant to the tumor was comparable to that in normal lungs (data not shown). To further probe the subpopulations of tumor-infiltrating and lung resident leukocytes, we extracted CD45+ cells from the tumor and lung, respectively, and characterized them by flow cytometry. As shown in Figure 4*C* (left panels), we found that the portion of CD45+ cells that display high forward and side scatter was increased in the tumors relative to normal lung tissue and that upon gating on these cells and staining for CD11b and GR1, we could specifically detect the accumulation of CD45+ Gr-1$^{med}$ CD11b$^{high}$ leukocytes in the tumors relative to normal lung (Fig. 4*C*; right panels). Interestingly, data from the literature suggest that such CD45+ Gr-1$^{med}$ CD11b$^{high}$ cells represent myeloid-derived suppressor cells, which can exert various immune suppressive properties in the tumor microenvironment.[29] More broadly, the accumulation of both fibroblasts and leukocytes in the tumor–stroma interface strongly supports the notion that our orthotopic tumor implantation model affords a powerful tool to dissect temporal tumor and stromal changes at a single cell level in distinct compartments of a growing tumor.

## 3LL Tumors Express a Distinct Milieu of Chemokines that may Implicate Tumor–Stroma Communications

In the next part of the article, we set out to identify tumor-expressed functional molecules that potentially participate in the interactions between tumor cells and the lung microenvironment. To this end, we first performed a whole genome gene-chip analysis comparing the genomic expression patterns of 3LL tumors to those of normal lung tissue and of 3LL cells growing in culture. Focusing on the intensity of chemokine mRNA expression in the gene chip, we defined four groups of chemokines: (1) chemokines whose mRNA expression is nearly absent both in cultured 3LL cells and in the lungs (CXCL2 and CXCL3); (2) chemokines whose mRNA is expressed by cultured 3LL cells but is absent in the lungs (CCL2 and CCL7); (3) chemokines whose mRNA is absent in cultured 3LL cells but is highly expressed in the lungs (CXCL12, CXCL16, and CCL5, also defined as lung homeostatic chemokines); and (4) chemokines whose mRNA levels are low in cultured 3LL cells but show intermediate expression in the lungs (CCL3, CCL17, and CCL22). We next assessed the expression of these chemokines by qPCR. As shown in Figure 5*A–D*, the mRNA of the myeloid cell attracting chemokines (CXCL2 and CXCL3) and the CCR2-binding chemokines (CCL2 and CCL7) was specifically induced in the tumor microenvironment, whereas the mRNA of the lung homeostatic chemokines (those whose mRNA is highly expressed in the normal lung: CXCL12, CXCL16, and CCL5) were suppressed in the tumors.[30–33]

To confirm that indeed the chemokines whose mRNA is up-regulated in the tumors were also produced in the tumor, we decided to focus on the two chemokines whose mRNA is most profoundly present in the tumors: CCL2 and CCL7. Using ELISA, we showed that high protein levels of both CCL2 and CCL7 were detected in the tumors relative to normal lung tissue (Fig. 5*E*). Notably, the protein levels of CCL2 and CCL7 in the tumor were much higher than in the blood of the tumor-bearing mice (2577 ± 159 pg/mg of protein versus 189 ± 25 pg/ml of blood for CCL2 and 1341 ± 67 pg/mg of protein versus 96 ± 22 pg/ml of blood for CCL2), thus suggesting that these chemokines may attract CCR2-expressing monocyte subpopulations to the tumor microenvironment.[30–33] In addition, the unique pattern of chemokine expression in the tumor demonstrates that the orthotopic tumor implantation approach avoids the induction of changes in gene expression in the entire lung microenvironment and restricts them to the confined area of the tumor.

## Upon Implantation in the Lung, Human Lung Cancer Cells Generate a Single Pulmonary Nodule that, Over Time, Locally Grows and Forms Metastasis

In the final part of the article, we tested the generalizability of our findings by investigating whether orthotopic

 

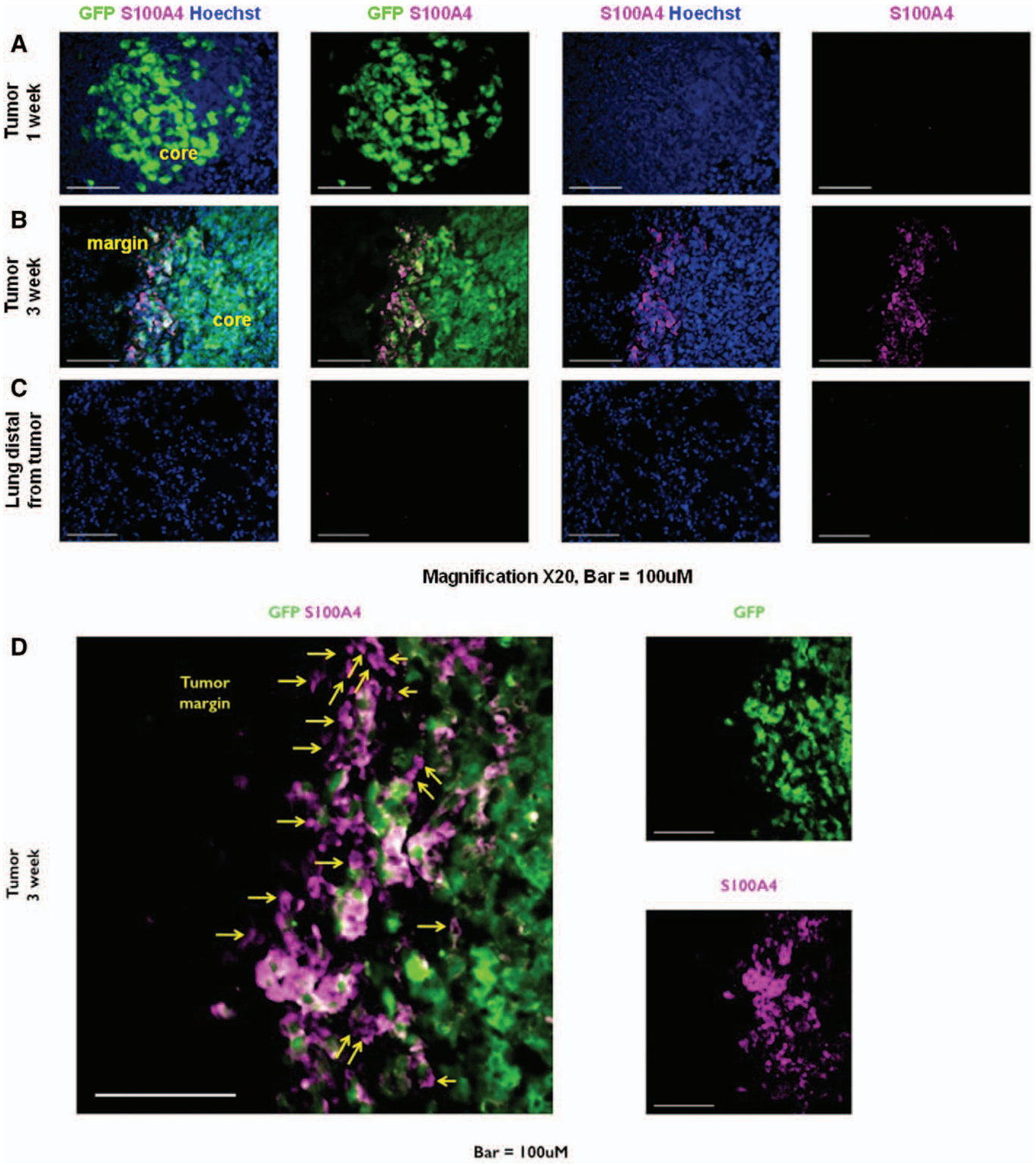


**FIGURE 3.** *A–C*, Fibroblast accumulation around 3LL tumors stained 1 and 3 weeks after implantation of 500 GFP-expressing 3LL cells. Green: anti-GFP staining, blue: Hoechst nuclear staining, purple: anti-S100A4. Magnification (×10), Bar = 100 μm. *A*, Representative 1-week tumor section; (*B*) representative 3-week tumor section showing both the margin and the core of the tumor; (*C*) representative 3-week lung section 3 mm distant from the primary tumor site with the same markers as in panels A and B. *D*, A magnified image of anti-GFP and anti-S100A4 staining, arrowheads point to S100A4-positive GFP-negative cells.

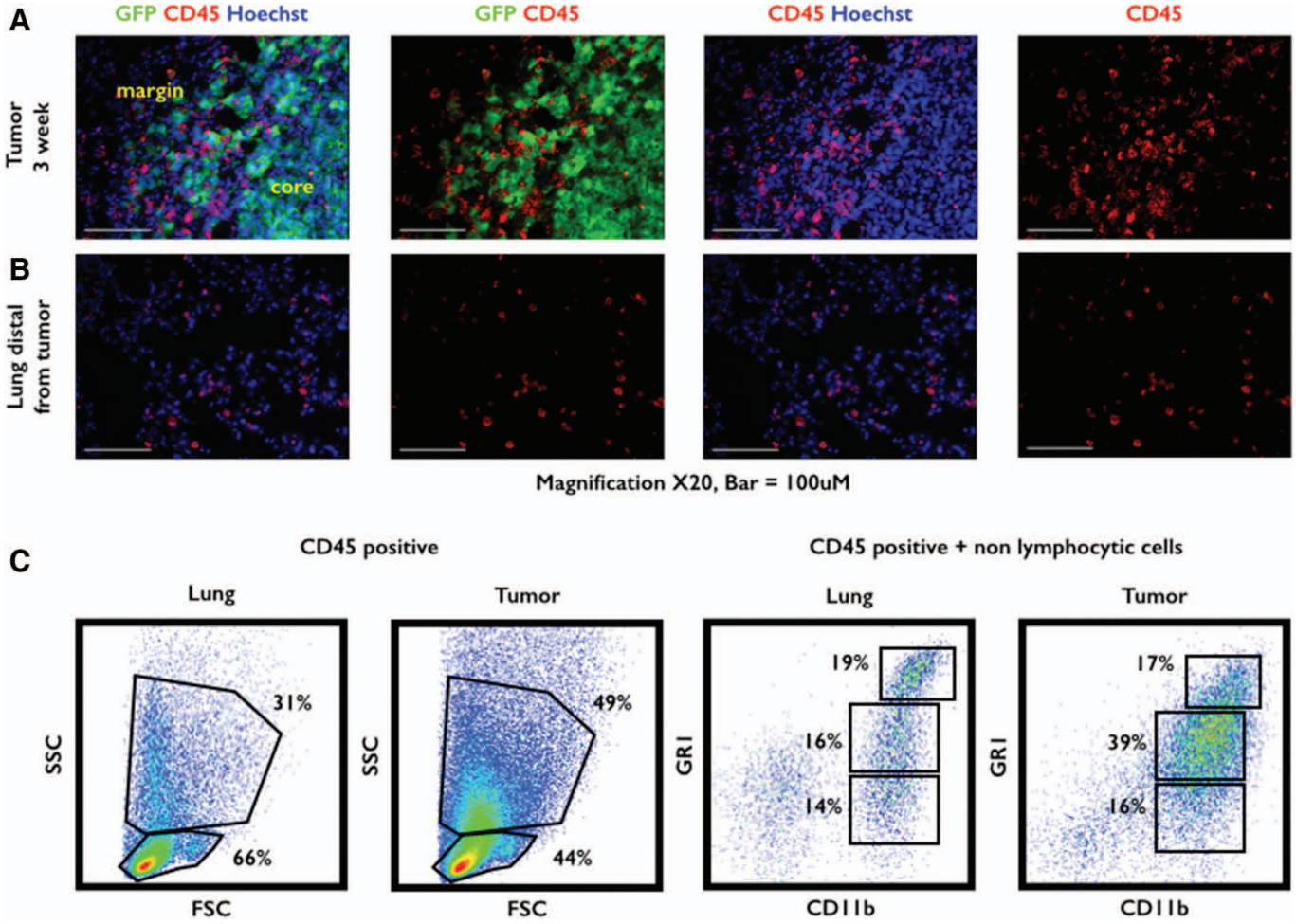


**FIGURE 4.** *A* and *B,* Immune cell accumulation around 3LL tumors stained 3 weeks after implantation of 500 GFP-expressing 3LL cells. Green: anti-GFP staining, blue: Hoechst nuclear staining, red: anti-CD45. Bar = 100 μm. *A,* Representative 3-week tumor section showing both the margin and the core of the tumor and (*B*) representative 3-week lung section 3 mm distant from the primary tumor site. *C,* Representative dot-plot analysis of the staining of lung- and tumor-derived immune cells (CD45-gated cells) for their forward and side scatter and for the cell surface markers CD11b and Gr-1 are shown. Two right panels: forwards/side scatter plots. Two left panels: CD11b/GR1 plots. The percentages of each population of cells out of total gated cells are shown.

delivery of small numbers of human lung cancer cells is applicable for generating human NSCLC tumors in immune-compromised recipient mice (NSG mice). In previously published works that have used orthotopic implantation of human NSCLC cells, researchers report the injection of very large number of cells ($10^6$–$10^7$) and portray the formation of a non-anatomically bound parenchymal, pleural, and mediastinal disease. To avoid these drawbacks, we decided to limit our injection to no more than $1 \times 10^4$ human lung carcinoma cells and to test two different human NSCLC cell lines: (1) the large cell carcinoma cell line H460 and (2) the adenocarcinoma cell line A549. Six weeks after the injection of $1 \times 10^4$ H460 cells, we killed the mice and found that tumors formed in 83% (5 of 6) of injected mice (Fig. 6*A*). Moreover, when sampling the contralateral lung and the liver of these tumor-bearing mice, we found that 66% (4 of 6) of mice developed lung metastasis (Fig. 6*B*) and 33% (2 of 6) developed liver metastasis (Fig. 6*C*). Notably, injection of a smaller number of H460 cells ($7.5 \times 10^3$) resulted in a slightly lower rate of tumor formation (4 of 6, 66.6%). Similarly, we observed that 6 weeks after injection of $5 \times 10^3$ A549 cells, 100% of the injected mice (5 of 5) developed lung tumors (Fig. 6*D*). In addition, 60% (3 of 5) of the A549 injected mice also developed distant lung metastasis (Fig. 6*B*) but none of the animals developed liver metastasis. Taken together, these observations demonstrate that orthotopic delivery of small numbers of human NSCLC is a suitable approach to induce solitary lung tumor implants and that this approach is also an attractive modeling system to mimic the metastatic spread of human lung cancer from the lung to secondary organs.

## DISCUSSION

The recent and ongoing emergence of lung cancer screening programs is anticipated to significantly increase the number of patients diagnosed with early-stage lung cancer.[34–36] This trend emphasizes the growing need for an

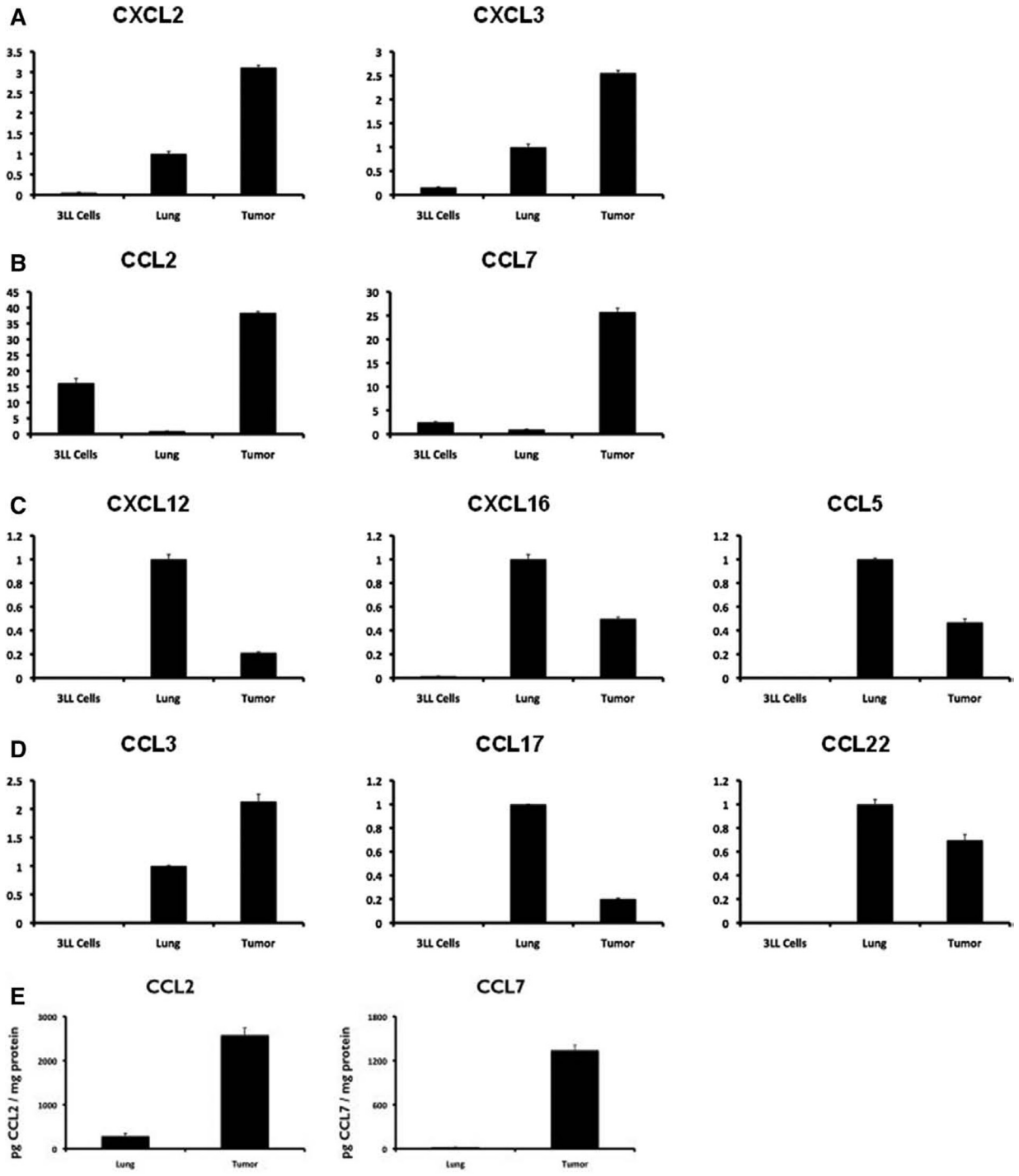


**FIGURE 5**. *A–D,* The fold increase or decrease in expression of mRNA for the chemokines CXCL-2, 3, 12, 16 and CCL-2, 3, 5, 7, 17, 22 in 3LL cells in vitro (3LL cells) and in 3LL tumors in vivo (tumor) relative to normal lungs in vivo (lung) is shown. The data were acquired using quantitative polymerase chain reaction, and the fold increase or decrease in chemokine expression is always presented relative to normal lung tissue. The chemokines in the figure are divided into four distinct groups of chemokine according to their relative mRNA expression in the native lung and in 3LL cells in culture. (This division is based on gene-chip data that we have analyzed and whose complete result is not shown here.) *A,* Chemokines whose mRNA expression is nearly absent both in cultured 3LL cells and in the lungs (CXCL2 and CXCL3); (*B*) chemokines whose mRNA is expressed by cultured 3LL cells but is absent in the lungs (CCL2 and CCL7); (*C*) chemokines whose mRNA is absent in cultured 3LL cells but is highly expressed in the lungs (CXCL12, CXCL16, CCL5, also defined as lung homeostatic chemokines); and (*D*) chemokines whose mRNA levels are low in cultured 3LL cells but show intermediate expression in the lungs (CCL3, CCL17, and CCL22). *E,* The CCL2 and CCL7 protein content (picograms of chemokine per milligrams of protein) in 3LL tumors and control normal lung parenchyma is shown.

 

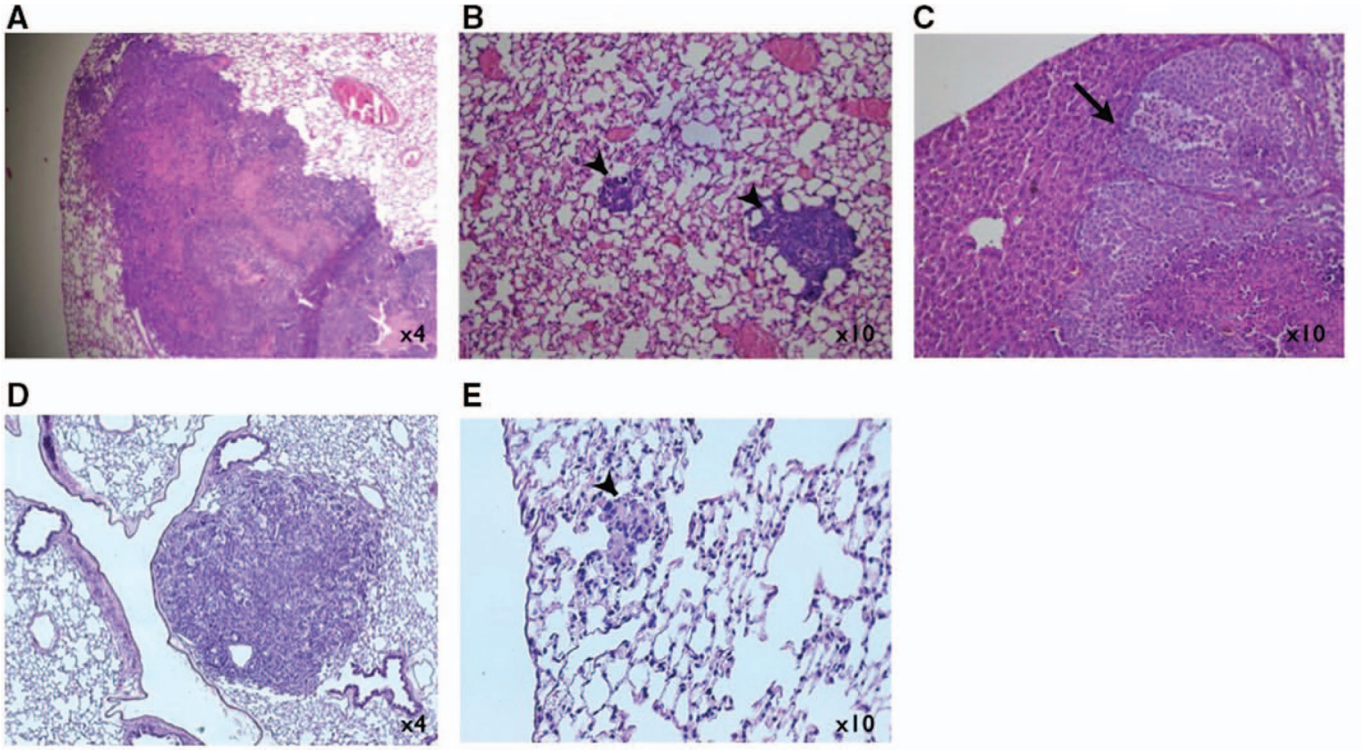


**FIGURE 6.** Representative histologic sections from the lungs and liver of an NSG mouse that was killed 6 weeks after injection of H460 and A549 cells into the left lung. *A,* H460 tumor in the left lung (magnification, ×4); (*B*) H460 micrometastasis in contralateral lung (magnification ×10); (*C*) H460 metastasis in the liver (magnification, ×10); (*D*) A549 tumor in the left lung (magnification, ×4); and (*E*) H460 distant micrometastasis (magnification, ×10).

accurate early-stage lung cancer modeling system that will allow researchers to follow the dynamics of cancer growth and spread in and from the native lung microenvironment, and consequently, facilitate the future discovery of key molecular mechanisms that govern disease progression.[4–6] In this article, we attempted to address this challenge and present a novel lung cancer model that is based on refined and accurate delivery of very small numbers of either human or murine lung cancer cells directly into the lung parenchyma. By implementing this technique, we were able to closely mimic in vivo the clinical sequence of events that characterize the propagation of early-stage human NSCLC. More specifically, using either human or murine lung cancer cells, the experimental methodology successfully induced a solitary microscopic pulmonary nodule that was surrounded by normal lung parenchyma and that during a follow-up period of 1 to 6 weeks locally grew and spread. Remarkably, we found that the syngeneic lung carcinoma tumors were highly invasive and also induced the accumulation of fibroblasts and distinct populations of infiltrating leukocytes in the tumor leading edge. Therefore, we suggest that our new model can provide a useful tool to investigate various levels of tumor cell communications both with the lung stroma and with lung-infiltrating leukocytes and that the model may shed light on the outcomes of these communications in regard of tumor growth and invasion. Finally, the ability of locally implanted human lung cancer cells to metastasize to secondary sites is analogous to the pathologic course of human NSCLC metastasis making our model useful for addressing the metastatic potential of human lung cancers and their in vivo susceptibility to anticancer drugs.

Notably, our findings contrast with previous attempts by several research groups, which as a result of the accelerated interest in recent years in the original tumor microenvironment have also tried to model lung cancer by directly injecting malignant cells to the lung parenchyma.[23,24,37–39] These initial attempts, made with both human and murine lung cancer cells, have reported important findings that have highlighted the significance of mimicking the disease in its native anatomic location.[12,39] Nonetheless, the methodology reported in these studies suffers from several major limitations that prevent the accurate mimicry of early-stage lung cancer. Indeed, unlike this article, these studies reported the injection of large numbers of tumor cells in relatively large volumes of cell suspensions (e.g., $>1 \times 10^6$ cells in 20 μl volume).[23,39] In addition, the researchers relied on large needles and syringes to inject their tumor cells.[24,37–39] As a result, for example, their technique lead both to the early spread of cells from the lung to the thorax in a manner that does not relate to the pathologic behavior of early-stage human lung cancer and to metastasis of the tumor to axillary lymph nodes that are not considered a primary site for metastasis of early-stage lung cancer.[23,39] The centrality of these limitations was further evident when we attempted to replicate these previously published methodologies in our own laboratory. Specifically, in our hands, we noticed that the use of large needles and large injection volumes was associated with excessive tissue damage and that the avoidance of

stereotactic guidance for injection made it difficult to assure the precise location and depth of tumor cell injection.

The methodology suggested in this article overcomes these critical technical considerations by utilizing smaller syringes, by dramatically reducing both the number of injected cells and the volume of cell suspension (i.e., 500 cells in 2 µl volume), and by introducing the cells under the guidance of a stereotactic injection system. As a result, we were also able to ensure the precise depth and location of injection and to establish a refined method of tumor cell implantation that avoids the early spread of tumor cells to the chest wall and to extra thoracic lymph nodes such as axillary nodes that are not often involved in early stages of NSCLC.[3] Indeed, to further solidify the anatomically confined nature of our injection methodology, evidence from GFP-tagged cells demonstrated that only a single tumor focus was formed after tumor cell injection and that no singular cancer cells were found distant to the original injection site. In addition, and unlike previous works, the histologic appearance of the lung tissue as early as 1 week after tumor cell implantation showed that the lung parenchyma surrounding the tumor was intact. Thus, we conclude that the technical modifications that we introduced allowed for the development of orthotopically induced tumors that recapitulate many important characteristics of early-stage human lung cancer.

By being able to better model malignant diseases in a manner that closely resembles clinical disease characteristics, both with regard to primary anatomic location and with regard to secondary sites of spread and metastasis, we propose that our orthotopic lung cancer modeling system has the potential to characterize distinct cellular and immunologic events that occur specifically in the tumor's microenvironment and that may represent the signature of pathologic processes that support the tumor's growth and spread.[7,9] Some intriguing evidence for this has been demonstrated in the latter part of the article, where we found, for example, that orthotopically implanted 3LL tumors induced the time-dependent accumulation of both fibroblast and leukocytes in the tumors expanding margin and that upon deeper probing of the tumor-associated leukocytes, a population of CD45+ Gr-1$^{med}$ CD11b$^{high}$ cells that may exhibit immune suppressive properties was detected specifically in the tumors relative to their surrounding normal lung parenchyma.[29,40] We further observed a specific profile of chemokines that were expressed by the tumor such that the myeloid cell attracting chemokines (CXCL2 and CXCL3) and the CCR2-binding chemokines (CCL2 and CCL7) were specifically up-regulated in the tumors relative to their surrounding normal lung parenchyma, whereas the homeostatic lung chemokines (CXCL12, CXCL16, and CCL5) were specifically down-regulated in the tumors.[30–33] Together, these findings sketch two potentially interesting tumor–stroma crosstalk pathways that may be involved in regulating lung cancer tumor growth and spread. First, the expression of the myeloid cell attracting chemokines (CXCL2 and CXCL3) in the tumors and the specific recruitment of CD45+ Gr-1$^{med}$ CD11b$^{high}$ cells to the tumors may represent an immune modulation mechanism that favors tumor growth.[29,40] Second, the expression of CCL7 and CCL2 in the tumors and the specific accumulation of fibroblasts at the tumor margin may represent a molecular and cellular signature to the invasive nature of the tumor.[41,42] Although these two pro-tumorogenic pathways which have been detected by our model require further validation, some initial evidence for the first proposition comes from previous publications which have reported that the knocking down of CXCL2 in metastatic breast cancer cells reduced the accumulation of myeloid suppressive cells in the tumor.[43,44] These studies have further demonstrated that the CXCR2/CXCL2/CXCL3 axis is tumorogenic.[43,44] Some support for the second proposition comes from research which has shown that cancer-associated fibroblast-derived CCL7 specifically promoted the invasion and migration of malignant cells. These researchers further showed that neutralizing the tumor receptors for CCL7 (CCR1, CCR2, and CCR3) may inhibit tumor cell migration.[41,42]

Importantly, we must acknowledge the inherent limitations of the immune-compromised model used by us for implanting human lung cancer cells rather than murine lung cancer cells in mice. In addition, we acknowledge that tumor growth may vary considerably between distinct types and protocols of implanted cells and mice hosts (e.g., immune status, strain, age, microbiota). And yet, the advantages of our orthotopic lung cancer models, which are based on delivery of small number of tumor cells directly into the lung parenchyma, are clear as these models more accurately mimic the clinical manifestation of early-stage human NSCLC. As such, we suggest that our model system represents an attractive platform to dissect key molecular mechanisms that govern not only lung tumor propagation and metastasis but also tumor resistance to drugs. We therefore anticipate that this and similar orthotopic models adapted for other types of tumors and organs will be highly attractive for studies on the efficacy of anticancer drugs under various clinically relevant settings.

## STATEMENT OF TRANSLATIONAL RELEVANCE

*The recent and ongoing emergence of lung cancer screening programs is anticipated to significantly increase the number of patients diagnosed with early-stage lung cancer. This trend emphasizes the growing need for an accurate early-stage lung cancer modeling system that will allow researchers to follow the dynamics of cancer growth and spread in and from the native lung microenvironment, and consequently, facilitate the future discovery of key molecular mechanisms that govern disease progression. In this article, we present a novel stereotactic-guided injection-based orthotopic lung cancer model that closely mimics the pathologic sequence of events that characterizes early-stage human lung cancer propagation. This model thus serves as an attractive platform to probe tumor–stromal cell interactions and to test therapeutic targets under conditions that reflect early-stage lung cancer.*

## ACKNOWLEDGMENT

*The authors thank the Cyclotron unit of Hadassah Medical Organization for providing 18F-FDG and imaging with micro-PET/CT. The authors thank Dr. C. Tadmor for her thoughtful comments and assistance in editing the manuscript.*

 

## REFERENCES


1. Siegel R, Naishadham D, Jemal A. Cancer statistics, 2012. *CA Cancer J Clin* 2012;62:10–29.
2. Siegel R, DeSantis C, Virgo K, et al. Cancer treatment and survivorship statistics, 2012. *CA Cancer J Clin* 2012;62:220–241.
3. Detterbeck FC, Boffa DJ, Tanoue LT. The new lung cancer staging system. *Chest* 2009;136:260–271.
4. Wald O, Shapira OM, Izhar U. CXCR4/CXCL12 axis in non small cell lung cancer (NSCLC) pathologic roles and therapeutic potential. *Theranostics* 2013;3:26–33.
5. Saintigny P, Burger JA. Recent advances in non-small cell lung cancer biology and clinical management. *Discov Med* 2012;13:287–297.
6. Burger JA, Stewart DJ, Wald O, Peled A. Potential of CXCR4 antagonists for the treatment of metastatic lung cancer. *Expert Rev Anticancer Ther* 2011;11:621–630.
7. Hanahan D, Weinberg RA. Hallmarks of cancer: the next generation. *Cell* 2011;144:646–674.
8. Chaffer CL, Weinberg RA. A perspective on cancer cell metastasis. *Science* 2011;331:1559–1564.
9. Perlikos F, Harrington KJ, Syrigos KN. Key molecular mechanisms in lung cancer invasion and metastasis: a comprehensive review. *Crit Rev Oncol Hematol* 2013;87:1–11.
10. Meuwissen R, Berns A. Mouse models for human lung cancer. *Genes Dev* 2005;19:643–664.
11. de Seranno S, Meuwissen R. Progress and applications of mouse models for human lung cancer. *Eur Respir J* 2010;35:426–443.
12. Graves EE, Vilalta M, Cecic IK, et al. Hypoxia in models of lung cancer: implications for targeted therapeutics. *Clin Cancer Res* 2010;16:4843–4852.
13. O'Hagan RC, Heyer J. KRAS mouse models: modeling cancer harboring KRAS mutations. *Genes Cancer* 2011;2:335–343.
14. Akopyan G, Bonavida B. Understanding tobacco smoke carcinogen NNK and lung tumorigenesis. *Int J Oncol* 2006;29:745–752.
15. Jackson EL, Olive KP, Tuveson DA, et al. The differential effects of mutant p53 alleles on advanced murine lung cancer. *Cancer Res* 2005;65:10280–10288.
16. Politi K, Pao W. How genetically engineered mouse tumor models provide insights into human cancers. *J Clin Oncol* 2011;29:2273–2281.
17. Zhou Y, Rideout WM 3rd, Zi T, et al. Chimeric mouse tumor models reveal differences in pathway activation between ERBB family- and KRAS-dependent lung adenocarcinomas. *Nat Biotechnol* 2010;28:71–78.
18. DuPage M, Dooley AL, Jacks T. Conditional mouse lung cancer models using adenoviral or lentiviral delivery of Cre recombinase. *Nat Protoc* 2009;4:1064–1072.
19. Frese KK, Tuveson DA. Maximizing mouse cancer models. *Nat Rev Cancer* 2007;7:645–658.
20. Wakamatsu N, Devereux TR, Hong HH, Sills RC. Overview of the molecular carcinogenesis of mouse lung tumor models of human lung cancer. *Toxicol Pathol* 2007;35:75–80.
21. Khong HT, Restifo NP. Natural selection of tumor variants in the generation of "tumor escape" phenotypes. *Nat Immunol* 2002;3:999–1005.
22. Fantozzi A, Christofori G. Mouse models of breast cancer metastasis. *Breast Cancer Res* 2006;8:212.
23. Liu X, Liu J, Guan Y, et al. Establishment of an orthotopic lung cancer model in nude mice and its evaluation by spiral CT. *J Thorac Dis* 2012;4:141–145.
24. Yamaura T, Doki Y, Murakami K, Saiki I. Model for mediastinal lymph node metastasis produced by orthotopic intrapulmonary implantation of lung cancer cells in mice. *Hum Cell* 1999;12:197–204.
25. Rock JR, Barkauskas CE, Cronce MJ, et al. Multiple stromal populations contribute to pulmonary fibrosis without evidence for epithelial to mesenchymal transition. *Proc Natl Acad Sci U S A* 2011;108:E1475–E1483.
26. Joyce JA, Pollard JW. Microenvironmental regulation of metastasis. *Nat Rev Cancer* 2009;9:239–252.
27. Chen N, Sato D, Saiki Y, Sunamura M, Fukushige S, Horii A. S100A4 is frequently overexpressed in lung cancer cells and promotes cell growth and cell motility. *Biochem Biophys Res Commun* 2014;447:459–464.
28. Takenaga K, Nakamura Y, Sakiyama S. Expression of antisense RNA to S100A4 gene encoding an S100-related calcium-binding protein suppresses metastatic potential of high-metastatic Lewis lung carcinoma cells. *Oncogene* 1997;14:331–337.
29. Montero AJ, Diaz-Montero CM, Kyriakopoulos CE, Bronte V, Mandruzzato S. Myeloid-derived suppressor cells in cancer patients: a clinical perspective. *J Immunother* 2012;35:107–115.
30. Zlotnik A, Yoshie O. Chemokines: a new classification system and their role in immunity. *Immunity* 2000;12:121–127.
31. Zlotnik A, Burkhardt AM, Homey B. Homeostatic chemokine receptors and organ-specific metastasis. *Nat Rev Immunol* 2011;11:597–606.
32. Balkwill FR. The chemokine system and cancer. *J Pathol* 2012;226:148–157.
33. Mantovani A, Schioppa T, Porta C, Allavena P, Sica A. Role of tumor-associated macrophages in tumor progression and invasion. *Cancer Metastasis Rev* 2006;25:315–322.
34. Jacobson FL, Austin JH, Field JK, et al. Development of The American Association for Thoracic Surgery guidelines for low-dose computed tomography scans to screen for lung cancer in North America: recommendations of The American Association for Thoracic Surgery Task Force for Lung Cancer Screening and Surveillance. *J Thorac Cardiovasc Surg* 2012;144:25–32.
35. Jacobson FL, Jaklitsch MT. Lung cancer screening trials: the United States and beyond. *J Thorac Cardiovasc Surg* 2012;144:S3–S6.
36. Jaklitsch MT, Jacobson FL, Austin JH, et al. The American Association for Thoracic Surgery guidelines for lung cancer screening using low-dose computed tomography scans for lung cancer survivors and other high-risk groups. *J Thorac Cardiovasc Surg* 2012;144:33–38.
37. Doki Y, Murakami K, Yamaura T, Sugiyama S, Misaki T, Saiki I. Mediastinal lymph node metastasis model by orthotopic intrapulmonary implantation of Lewis lung carcinoma cells in mice. *Br J Cancer* 1999;79:1121–1126.
38. Koizumi K, Kozawa Y, Ohashi Y, et al. CCL21 promotes the migration and adhesion of highly lymph node metastatic human non-small cell lung cancer Lu-99 in vitro. *Oncol Rep* 2007;17:1511–1516.
39. Onn A, Isobe T, Itasaka S, et al. Development of an orthotopic model to study the biology and therapy of primary human lung cancer in nude mice. *Clin Cancer Res* 2003;9:5532–5539.
40. Gabrilovich DI, Ostrand-Rosenberg S, Bronte V. Coordinated regulation of myeloid cells by tumours. *Nat Rev Immunol* 2012;12:253–268.
41. Jung DW, Che ZM, Kim J, et al. Tumor-stromal crosstalk in invasion of oral squamous cell carcinoma: a pivotal role of CCL7. *Int J Cancer* 2010;127:332–344.
42. Mishra P, Banerjee D, Ben-Baruch A. Chemokines at the crossroads of tumor-fibroblast interactions that promote malignancy. *J Leukoc Biol* 2011;89:31–39.
43. Acharyya S, Oskarsson T, Vanharanta S, et al. A CXCL1 paracrine network links cancer chemoresistance and metastasis. *Cell* 2012;150:165–178.
44. Bachmeier BE, Mohrenz IV, Mirisola V, et al. Curcumin downregulates the inflammatory cytokines CXCL1 and -2 in breast cancer cells via NFkappaB. *Carcinogenesis* 2008;29:779–789.